AIMS Mathematics, 11(1): 1857–1877.
DOI: 10.3934/math.2026077
Received: 08 November 2025
Revised: 28 December 2025
Accepted: 14 January 2026
Published: 20 January 2026

https://www.aimspress.com/journal/Math

Research article

Primary resonance suppression in spur gear systems using hybrid proportional and fractional-order derivative displacement feedback control

Zhongyang Su[1], **Zhoujin Cui**[2,*] **and Hanlin Huang**[2]

[1] Jiangsu Maritime Institute, Nanjing, 211170, China

[2] School of Mathematical Sciences, Jiangsu Second Normal University, Nanjing, 210013, China

* **Correspondence:** Email: cuizhoujin@126.com.

Abstract: This paper investigated primary resonance suppression in nonlinear spur gear systems using a hybrid proportional and fractional-order derivative displacement feedback (P-FDDF) controller. The dynamic model of the system was established through a second-order non-autonomous differential equation incorporating time-varying meshing stiffness, backlash, and external excitations. The amplitude-frequency response equation of primary resonance was derived via the multiple scale method, while Lyapunov stability theory was employed to analyze the stability of steady-state solutions. Numerical analyses examined the effects of meshing damping, load fluctuations, meshing stiffness variations, and control parameters on resonance characteristics. Time history responses and phase diagrams demonstrated that the P-FDDF strategy achieves simultaneous resonant amplitude suppression and frequency tuning. The fractional-order component's frequency-weighting and memory properties enhance adaptability to complex nonlinear dynamics induced by time-varying meshing stiffness and backlash, establishing the P-FDDF as a reliable solution for gear system vibration control.

Keywords: hybrid control; primary resonance suppression; spur gear systems; fractional-order control; multiple scale method; amplitude-frequency response
Mathematics Subject Classification: 34A08, 70K42, 93C95

1. Introduction

Gear mechanisms are the most widely used transmission components, indispensable in applications ranging from simple mechanical equipment to complex industrial systems such as automobiles, aircraft, ships, and industrial robots [1,2]. Among various gear types, spur gear systems are favored for their compact structure and high efficiency, making them one of the most prevalent configurations in practical applications [3,4]. The dynamic behavior of these systems, particularly their vibrations, not

only directly determines operational stability but also significantly affects durability and performance. Consequently, understanding and controlling these vibrational characteristics has become a key focus in both powertrain engineering and nonlinear dynamics research [5, 6].

Given the critical impact of these vibrational properties on gear system performance, numerous studies have systematically investigated the influencing factors. For instance, Howard et al. developed a simplified gear dynamic model incorporating finite element-derived torsional mesh stiffness variations to examine friction's substantial impact on gear system vibration patterns [7]. Liu et al. employed advanced perturbation methods to analyze nonlinear parametric excitation dynamics in two-stage intermediate shaft gear systems [8, 9], while Yang et al. established a comprehensive single-degree-of-freedom model that integrates backlash, time-varying mesh stiffness, and multi-harmonic excitation to investigate multi-frequency excited nonlinear vibrations [10]. The importance of understanding these vibrational characteristics is further underscored by Moradi et al.'s work, which revealed critical phenomena such as jumping and instability in primary, superharmonic, and subharmonic resonances in clearance-containing spur cylindrical gear systems [11]. Additionally, comprehensive experimental and theoretical studies [12–15] have systematically examined spur gear system dynamics, covering essential aspects including backlash-related time-varying stiffness, tooth root crack-induced tribo-dynamical characteristics, subharmonic resonances, and dynamic performance during hovering maneuver flights. These collective investigations highlight the fundamental importance of vibration analysis in ensuring optimal design and reliable operation of gear transmission systems.

Building on the insights into gear system vibrational characteristics and their critical impacts, researchers have shifted focus to developing effective vibration control strategies for nonlinear gear systems. In terms of vibration control for such nonlinear gear systems, relevant studies have explored various active control strategies. Chen et al. proposed an active vibration reduction method for gear transmission by adjusting mesh stiffness and verified its effectiveness [16]. Li et al. developed a method to suppress gear transmission vibration by actively controlling the vibration of gear rotor support devices using piezoelectric stack devices, with experimental validation of its control performance [17]. Additionally, feedback control has emerged as a versatile tool for vibration suppression across a wide range of mechanical and structural systems, from spur gear transmissions and cantilever-beam dynamical systems to nonlinear motorcycle suspension schemes [18–23]. For example, in order to reduce vibration in spur gear systems, a time-delay feedback vibration reduction dynamic model of spur gears was established in [20], and the multiple scale method was applied to solve the time-delay feedback gear transmission system.

In recent years, fractional calculus and its applications have developed rapidly. Among various control methods, fractional-order control stands out for its superior adaptability in handling complex nonlinear dynamics compared to integer-order methods, making it a promising candidate for enhancing control performance [24–29]. However, despite the advancements in the aforementioned active control strategies and the potential of fractional-order control, several critical issues remain unresolved. Specifically, the potential of fractional-order control in addressing the nonlinear dynamics of spur gear systems has not been fully explored, and the synergistic effects of combining proportional control with fractional derivative control to simultaneously tune resonance frequency and suppress amplitudes remain underexamined. Furthermore, drawing inspiration from the above literature, this study intends to propose a hybrid proportional and fractional-order derivative displacement feedback (P-FDDF)

controller to suppress primary resonance in nonlinear spur gear systems.

The structure of this paper is as follows: Section 2 introduces the mathematical modeling of the spur gear system, including the dynamic equations with and without control, and details the derivation of the amplitude-frequency equation using the multiple scale method. Section 3 analyzes how various key parameters influence primary resonance characteristics through numerical simulations, including meshing damping, load fluctuations, meshing stiffness fluctuations and control parameters. Section 4 presents time history and phase diagram analyses to further validate the effectiveness of the P-FDDF controller by comparing the system's dynamic behaviors under controlled and uncontrolled conditions. Finally, Section 5 summarizes the main findings and presents the conclusions of the study.

2. Mathematical analysis

2.1. Mathematical modeling

To characterize the nonlinear dynamic behavior of a spur gear system, a simple torsional model of a gear pair is employed, as shown in Figure 1. Based on the formulation in [20], the model is described by the following second-order nonlinear differential equation that includes both constant and harmonic excitations:

$$\ddot{x} + \mu\dot{x} + (1 + k\cos\omega t)(d_1 x + d_2 x^3) = f_0 + f\cos\omega t, \tag{2.1}$$

where x denotes the differential value between dynamic and static transmission errors and is inherently displacement-related, as transmission errors in gear systems manifest as displacement-associated quantities. μ is the mesh damping coefficient, $1 + k\cos\omega t$ represents the time-varying mesh stiffness, k is the fluctuation amplitude of time-varying meshing stiffness, ω is the equivalent excitation frequency, $d_1 x + d_2 x^3$ is the backlash function which is used to represent gear clearances, f_0 is the equivalence static load, $f\cos\omega t$ is the equivalent dynamic load, and f is the amplitude of load fluctuation.

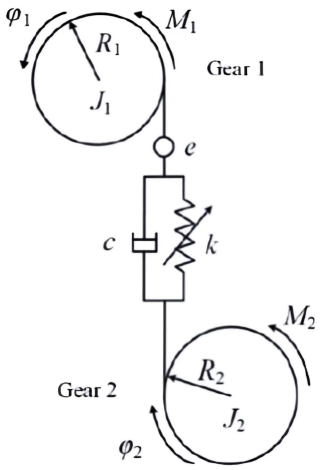

Figure 1. Dynamic model of a spur gear system [10].

Note that in the adopted model (2.1), the identical frequency of the time-varying mesh stiffness and equivalent dynamic load reflects a practical scenario where both excitations originate primarily from

the gear rotational motion. This modeling simplification focuses the analysis on primary resonance, which is the core objective of this study.

Under certain conditions, primary resonance with limited amplitude occurs in (2.1) when $\omega = \omega_0 \overset{\text{def}}{=} \sqrt{d_1}$ or $\omega \approx \omega_0$. To reduce vibrations in a spur gear system induced by external load fluctuations and time-varying meshing stiffness, a dynamic model incorporating time-delay feedback control was also established in [20], expressed as follows:

$$\ddot{x} + \mu\dot{x} + (1 + k\cos\omega t)(d_1 x + d_2 x^3) = f_0 + f\cos\omega t + g_1 x(t - \tau_d) + g_1\dot{x}(t - \tau_v). \tag{2.2}$$

While time-delay feedback control offers implementation simplicity and low computational demand by utilizing delayed error signals without complex modeling, certain limitations should be noted. The inherent time lag may compromise stability, particularly during high-speed operation or under variable loading conditions. Furthermore, its effectiveness is constrained when addressing nonlinear system characteristics such as backlash, meshing stiffness variations, and high-frequency vibrations, potentially impacting overall robustness. To address these issues and suppress vibrations in the spur gear system, we adopted a P-FDDF controller. Its closed-loop configuration is illustrated in Figure 2, and the specific expression of this control strategy is as follows:

$$\ddot{x} + \mu\dot{x} + (1 + k\cos\omega t)(d_1 x + d_2 x^3) = f_0 + f\cos\omega t - K_1 x(t) - K_2 D_t^q x(t), \tag{2.3}$$

where K_1 is the proportional displacement feedback control gain, and K_2 is the fractional-order derivative displacement feedback control gain. $D_t^q x(t)$ with $0 < q \leq 1$ is Caputo's fractional derivative of $x(t)$ described by

$$D_t^q x(t) = \frac{1}{\Gamma(1-q)} \int_0^t \dot{x}(s)(t-s)^{-q} \mathrm{d}s,$$

in which $\Gamma(z)$ denotes the Euler gamma function, satisfying the recursive property $\Gamma(z+1) = z\Gamma(z)$.

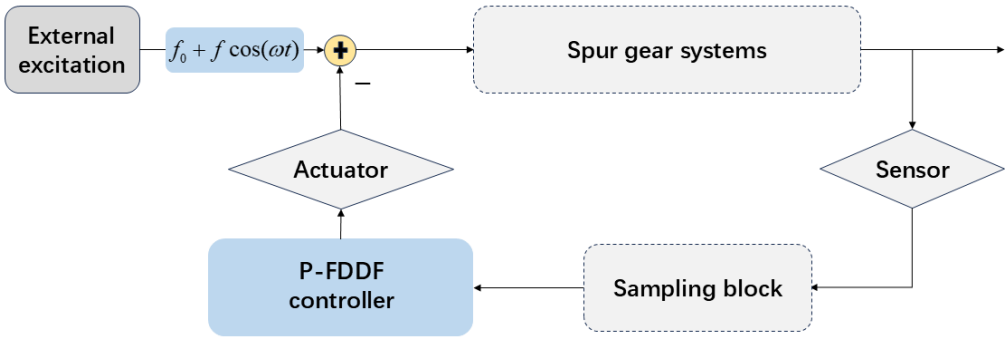

Figure 2. Closed-loop block diagram of the P-FDDF control strategy.

The adoption of the P-FDDF controller in spur gear systems is motivated by its ability to effectively address nonlinear resonant dynamics. The fractional-order component in the P-FDDF controller exhibits frequency-dependent weighting characteristics and long-memory properties, allowing it to adapt better to complex dynamics such as multi-frequency resonances. Additionally, the P-FDDF controller simplifies controller design via decoupled design parameters, facilitating calibration across

diverse operating conditions. Importantly, by directly targeting displacement-related transmission errors, it achieves suppression of transient and steady-state resonant vibrations associated with such errors, avoiding the phase distortions typical of time-delay approaches. These features make the P-FDDF controller a more reliable and high-performance solution for precise primary resonance suppression in spur gear systems.

2.2. Amplitude-frequency equation

In this study, following the classical framework of the multiple scale method, the amplitude-frequency equation of the controlled spur gear system is derived, adhering to the standard procedure described in the foundational references [30–32]. As a well-established tool for solving amplitude equations in nonlinear vibration analysis, the multiple scale method is based on the core idea of decomposing the system response into functions of distinct time scales for primary resonance analysis.

To apply this method for theoretical analysis, a small scaling parameter ε is first introduced. New time variables are then defined as $T_n = \varepsilon^n t$ $(n = 0, 1, \ldots)$. Consequently, the approximate solution of Eq (2.3) with small amplitudes can be expressed as

$$x(t, \varepsilon) = x_0(T_0, T_1, \ldots) + \varepsilon x_1(T_0, T_1, \ldots) + \cdots . \tag{2.4}$$

In this study, T_0 and T_1 are considered to obtain the first-order uniform solution to $O(\varepsilon)$.

The derivatives with respect to t can be expressed in terms of the new scaled times T_n as a series of partial derivatives:

$$\frac{\mathrm{d}}{\mathrm{d}t} = \frac{\partial}{\partial T_0}\frac{\mathrm{d}T_0}{\mathrm{d}t} + \frac{\partial}{\partial T_1}\frac{\mathrm{d}T_1}{\mathrm{d}t} + \cdots = D_0 + \varepsilon D_1 + \cdots , \tag{2.5a}$$

$$\frac{\mathrm{d}^2}{\mathrm{d}t^2} = D_0^2 + 2\varepsilon D_0 D_1 + \varepsilon^2 D_1^2 + \cdots , \tag{2.5b}$$

$$D_t^q = D_0^q + q\varepsilon D_0^{q-1} D_1 + \cdots , \tag{2.5c}$$

in which $D_0^q = \frac{\partial^q}{\partial T_0^q}$, $D_n = \frac{\partial}{\partial T_n}$, $D_n^2 = \frac{\partial^2}{\partial T_n^2}$ $(n = 0, 1)$.

Moreover, for such a small parameter ε, the mesh damping, mesh stiffness, nonlinear term, excitation load, and control gains must be ordered at the same level of approximation by letting

$$\mu \to \varepsilon\mu, \quad k \to \varepsilon k, \quad d_2 \to \varepsilon d_2, \quad f \to \varepsilon f, \quad K_1 \to \varepsilon K_1, \quad K_2 \to \varepsilon K_2. \tag{2.6}$$

By scaling these parameters to the same order of ε, the amplitude of load fluctuation, damping, nonlinear terms, and feedback control gains are retained in the same perturbation equation, such that a uniformly valid asymptotic solution can be derived. This approach enables a comprehensive analysis of the system's dynamic behavior in the vicinity of parametric resonance.

Then, Eq (2.3) becomes

$$\ddot{x} + \varepsilon\mu\dot{x} + (1 + \varepsilon k\cos\omega t)(d_1 x + \varepsilon d_2 x^3) = f_0 + \varepsilon f\cos\omega t - \varepsilon K_1 x(t) - \varepsilon K_2 D_t^q x(t). \tag{2.7}$$

The resonance relation is considered as $\omega = \omega_0 \overset{\text{def}}{=} \sqrt{d_1}$ or $\omega \approx \omega_0$, and a detuning parameter σ describing the nearness of ω to ω_0 is introduced by

$$\omega = \omega_0 + \varepsilon\sigma. \tag{2.8}$$

Then, $\omega t = \omega_0 T_0 + \sigma T_1$. Substituting (2.4), (2.5a)–(2.5c) into (2.3), equating the coefficients of the same power of ε, a set of linear differential equations is obtained:

$$O(\varepsilon^0) : D_0^2 x_0 + \omega_0^2 x_0 = f_0, \tag{2.9}$$

$$\begin{aligned} O(\varepsilon^1) : D_0^2 x_1 + \omega_0^2 x_1 = &- 2D_0 D_1 x_0 - \mu D_0 x_0 - d_2 x_0^3 - K_1 x_0 - K_2 D_0^q x_0 \\ &- \omega_0^2 k x_0 \cos(\omega T_0 + \sigma T_1) + f \cos(\omega T_0 + \sigma T_1), \end{aligned} \tag{2.10}$$

from which x_0 and x_1 can be solved individually. In this way, the resonant solution x is dominated by x_0, complemented by εx_1.

The general solution of Eq (2.9) is of the form

$$x_0 = A(T_1)\mathrm{e}^{\mathrm{i}\omega_0 T_0} + \overline{A}(T_1)\mathrm{e}^{-\mathrm{i}\omega_0 T_0} + \Lambda, \tag{2.11}$$

where $A(T_1)$ and $\overline{A}(T_1)$ are unknown functions, $\overline{A}(T_1)$ denotes the complex conjugate of $A(T_1)$, $\Lambda = \frac{f_0}{\omega_0^2}$.

Substituting (2.11) into Eq (2.10), and using the following two formulas [33–35],

$$D_t^q \mathrm{e}^{\mathrm{i}\omega t} \approx (\mathrm{i}\omega)^q \mathrm{e}^{\mathrm{i}\omega t}, \quad \cos(\omega_0 T_0 + \sigma T_1) = \frac{\mathrm{e}^{\mathrm{i}(\omega_0 T_0 + \sigma T_1)} + \mathrm{e}^{-\mathrm{i}(\omega_0 T_0 + \sigma T_1)}}{2},$$

the right-hand side of Eq (2.10) becomes

$$[-2\mathrm{i}\omega_0 D_1 A - \mathrm{i}\omega_0 \mu A - 3d_2 A^2 \bar{A} - 3d_2 \Lambda^2 A - K_1 A - K_2 A(\mathrm{i}\omega_0)^q + \frac{f - \omega_0^2 k\Lambda}{2}\mathrm{e}^{\mathrm{i}\sigma T_1}]\mathrm{e}^{\mathrm{i}\omega_0 T_0} + NST + cc, \tag{2.12}$$

where NST stands for the terms that do not produce secular terms and cc denotes the complex conjugate of the preceding terms.

To eliminate the secular term from Eq (2.12), the following equation should be satisfied:

$$2\mathrm{i}\omega_0 D_1 A + \mathrm{i}\omega_0 \mu A + 3d_2 A^2 \bar{A} + 3d_2 \Lambda^2 A + K_1 A + K_2 A(\mathrm{i}\omega_0)^q - \frac{f - \omega_0^2 k\Lambda}{2}\mathrm{e}^{\mathrm{i}\sigma T_1} = 0. \tag{2.13}$$

With the help of the Euler formula

$$\mathrm{i}^q = (\mathrm{e}^{\mathrm{i}\pi/2})^q = \mathrm{e}^{\mathrm{i}q\pi/2} = \cos\frac{q\pi}{2} + \mathrm{i}\sin\frac{q\pi}{2}, \tag{2.14}$$

substituting the estimations $A(T_1) = \frac{a(T_1)}{2}\mathrm{e}^{\mathrm{i}\theta(T_1)}$, $\varphi(T_1) \overset{\text{def}}{=} \sigma T_1 - \theta(T_1)$, by separating the real and imaginary parts of Eq (2.13), the differential equations governing amplitude $a(T_1)$ and $\varphi(T_1)$ of $A(T_1)$ are expressed as

$$D_1 a = -\frac{K_2 a}{2}\omega_0^{q-1}\sin\frac{q\pi}{2} - \frac{\mu a}{2} + \frac{f - \omega_0^2 k\Lambda}{2\omega_0}\sin\varphi, \tag{2.15a}$$

$$aD_1\varphi = \sigma a - \frac{K_2 a}{2}\omega_0^{q-1}\cos\frac{q\pi}{2} - \frac{K_1 + 3d_2\Lambda^2}{2\omega_0}a - \frac{3d_2}{8\omega_0}a^3 + \frac{f - \omega_0^2 k\Lambda}{2\omega_0}\cos\varphi. \tag{2.15b}$$

By letting $D_1 a = 0$ and $D_1\varphi = 0$ in Eqs (2.15a) and (2.15b), the steady-state motions can be written as

$$-\frac{K_2 a}{2}\omega_0^{q-1}\sin\frac{q\pi}{2} - \frac{\mu a}{2} = -\frac{f - \omega_0^2 k\Lambda}{2\omega_0}\sin\varphi, \tag{2.16a}$$

$$\sigma a - \frac{K_2 a}{2}\omega_0^{q-1}\cos\frac{q\pi}{2} - \frac{K_1 + 3d_2\Lambda^2}{2\omega_0}a - \frac{3d_2}{8\omega_0}a^3 = -\frac{f - \omega_0^2 k\Lambda}{2\omega_0}\cos\varphi. \tag{2.16b}$$

Squaring and adding these two equations, the following amplitude-frequency response equation is determined:

$$[(\frac{\mu}{2} + \frac{K_2}{2}\omega_0^{q-1}\sin\frac{q\pi}{2})^2 + (\sigma - \frac{K_2}{2}\omega_0^{q-1}\cos\frac{q\pi}{2} - \frac{K_1 + 3d_2\Lambda^2}{2\omega_0} - \frac{3d_2}{8\omega_0}a^2)^2]a^2 = (\frac{f - \omega_0^2 k\Lambda}{2\omega_0})^2. \tag{2.17}$$

Specifically, when all control gains are set to zero, i.e., $K_1 = K_2 = 0$, the amplitude-frequency response equation under uncontrolled conditions can be derived, which is expressed as follows:

$$[\frac{\mu^2}{4} + (\sigma - \frac{3d_2\Lambda^2}{2\omega_0} - \frac{3d_2}{8\omega_0}a^2)^2]a^2 = (\frac{f - \omega_0^2 k\Lambda}{2\omega_0})^2. \tag{2.18}$$

The real solution a of Eq (2.18) determines the dominant part x_0 of the primary resonance response amplitude. The maximum amplitude $a_{\max}$ of the response curve derived from Eq (2.18) is

$$|a| \le a_{\max} \overset{\text{def}}{=} \left|\frac{f - \omega_0^2 k\Lambda}{\omega_0\mu}\right|. \tag{2.19}$$

It should be noted that the results of Eq (2.18) correct some errors in the amplitude-frequency response equations presented in [10, 20], where incorrect results were obtained in calculating the solution to Eq (2.9). This correction enhances the accuracy of the theoretical model and provides a more reliable basis for subsequent analysis.

2.3. Stability of the steady resonant solutions

To conclude this section, Lyapunov stability theory is employed to examine the stability of steady-state solutions. This mathematical framework, devised by Aleksandr Lyapunov in the late 19th century, serves as a key tool for assessing the stability of dynamical systems. It comprises two main strategies: The first (indirect) method and the second (direct) method of Lyapunov [36]. Here, we opt for the first method, which entails linearizing the system around its equilibrium point and evaluating the eigenvalues of the resulting Jacobian matrix. The equilibrium is asymptotically stable when all eigenvalues have negative real parts; it is unstable when any eigenvalue possesses a positive real part; and when eigenvalues have zero real parts, further analysis (like applying center manifold theory) is required to judge stability.

Assume that $(a, \varphi) = (a^*, \varphi^*)$ is a steady solution of Eqs (2.15a) and (2.15b), and let $\Delta a = a - a^*$ and $\Delta\varphi = \varphi - \varphi^*$. According to Eqs (2.16a) and (2.16b), the linearized differential equations governing Δa and $\Delta\varphi$ are

$$D_1\Delta a = -[\frac{K_2}{2}\omega_0^{q-1}\sin\frac{q\pi}{2} + \frac{\mu}{2}]\Delta a + \frac{f - \omega_0^2 k\Lambda}{2\omega_0}\cos\varphi^*\,\Delta\varphi, \tag{2.20a}$$

$$D_1\Delta\varphi = [\frac{\sigma}{a^*} - \frac{K_2}{2a^*}\omega_0^{q-1}\cos\frac{q\pi}{2} - \frac{K_1 + 3d_2\Lambda^2}{2\omega_0 a^*} - \frac{9d_2}{8\omega_0}a^*]\Delta a - \frac{f - \omega_0^2 k\Lambda}{2\omega_0 a^*}\sin\varphi^*\,\Delta\varphi. \tag{2.20b}$$

Let

$$P = \frac{K_2}{2}\omega_0^{q-1}\sin\frac{q\pi}{2} + \frac{\mu}{2}, \quad M = \sigma - \frac{K_2}{2}\omega_0^{q-1}\cos\frac{q\pi}{2} - \frac{K_1 + 3d_2\Lambda^2}{2\omega_0} - \frac{3d_2}{8\omega_0}(a^*)^2,$$

$$N = \sigma - \frac{K_2}{2}\omega_0^{q-1}\cos\frac{q\pi}{2} - \frac{K_1 + 3d_2\Lambda^2}{2\omega_0} - \frac{9d_2}{8\omega_0}(a^*)^2,$$

and then the characteristic equation can be rewritten as

$$\begin{vmatrix} -P-\lambda & -a^*M \\ \frac{1}{a^*}N & -P-\lambda \end{vmatrix} = 0. \tag{2.21}$$

By expanding the determinant, one has

$$\lambda^2 + 2P\lambda + (P^2 + MN) = 0. \tag{2.22}$$

Consider when $P > 0$, where the steady solution $(a, \varphi) = (a^*, \varphi^*)$ is asymptotically stable if and only if $P^2 + MN > 0$.

3. Analysis of the primary resonance characteristics

To investigate the vibration characteristics of spur gear systems, this section analyzes the effects of meshing damping, load fluctuations, meshing stiffness fluctuations, and control parameters on the primary resonance of such systems. This can be understood from the amplitude-frequency equation (2.17), which is rewritten here in terms of the original system parameters as follows:

$$[(\frac{\mu}{2} + \frac{K_2}{2}\omega_0^{q-1}\sin\frac{q\pi}{2})^2 + (\omega - \omega_0 - \frac{K_2}{2}\omega_0^{q-1}\cos\frac{q\pi}{2} - \frac{K_1 + 3d_2\Lambda^2}{2\omega_0} - \frac{3d_2}{8\omega_0}a^2)^2]a^2 = (\frac{f - \omega_0^2 k\Lambda}{2\omega_0})^2. \tag{3.1}$$

The effect of different parameters on the amplitude of the resonant solutions is investigated numerically.

In the parameter study of the simplified gear transmission system, the basic parameters of the selected spur gear sample are sourced from [20]. The initial dimensionless parameters of Eq (3.1) are defined based on the physical parameters of the system as follows: The meshing damping $\mu = 0.1$, the fluctuation amplitude of time-varying meshing stiffness $k = 0.2$, the dimensionless static load $f_0 = 0.1$, and the amplitude of dynamic load $f = 0.3$.

3.1. The influence of meshing damping

In the absence of feedback effects, i.e., $K_1 = 0, K_2 = 0$, the influence of meshing damping on the primary resonance is illustrated in Figure 3, which depicts the amplitude-frequency relationship of the gear system under different damping coefficients. In Figure 3(a), as μ increases, the nonlinear jump behavior of the system weakens and the resonance amplitude decreases. In other words, larger values of μ lead to a reduction in the unstable regions of the system. This indicates that the damping coefficient μ is a critical parameter in spur gear systems: The smaller the damping coefficient, the higher the amplitude of vibration during resonance. Figure 3(b) illustrates that when ω exceeds the primary resonance frequency and enters the unstable frequency band, a multi-valued phenomenon emerges, which in turn leads to system instability.

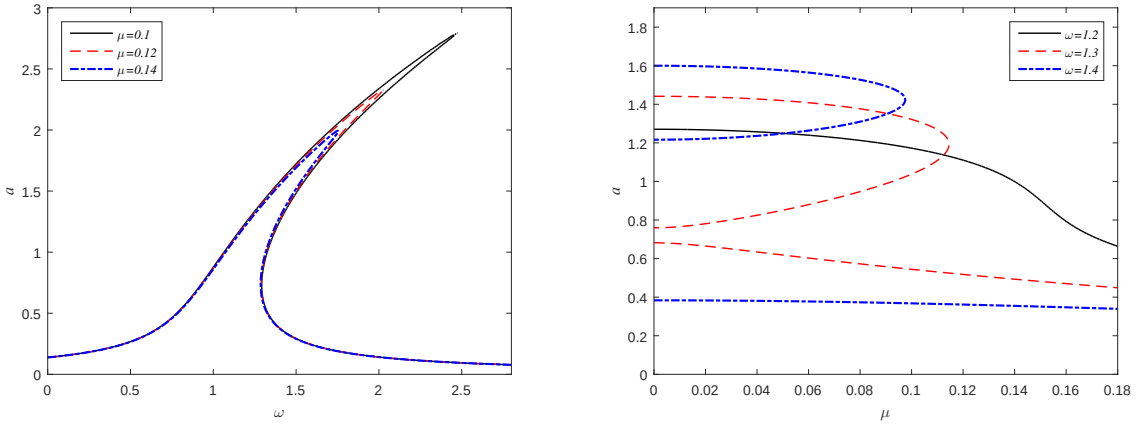

(a) (b)

Figure 3. Effect of the damping coefficient μ on the amplitude-frequency curves when $\omega_0 = 1$, $d_2 = 0.5$.

It is noteworthy that meshing damping is not a fixed parameter but can be adjusted in practice through methods like lubrication optimization or structural design, which underscores its practical significance as a key parameter for resonance control.

3.2. The influence of load fluctuations

When feedback effects are absent, the impact of load fluctuations on primary resonance is depicted in Figure 4. In Figure 4(a), with the increase of the load fluctuation f, the nonlinear jump behavior of the system becomes more pronounced, accompanied by an expansion of the resonance range and an increase in resonance amplitude. Additionally, Figure 4(b) reveals the presence of multiple amplitude branches as they enter the unstable frequency band.

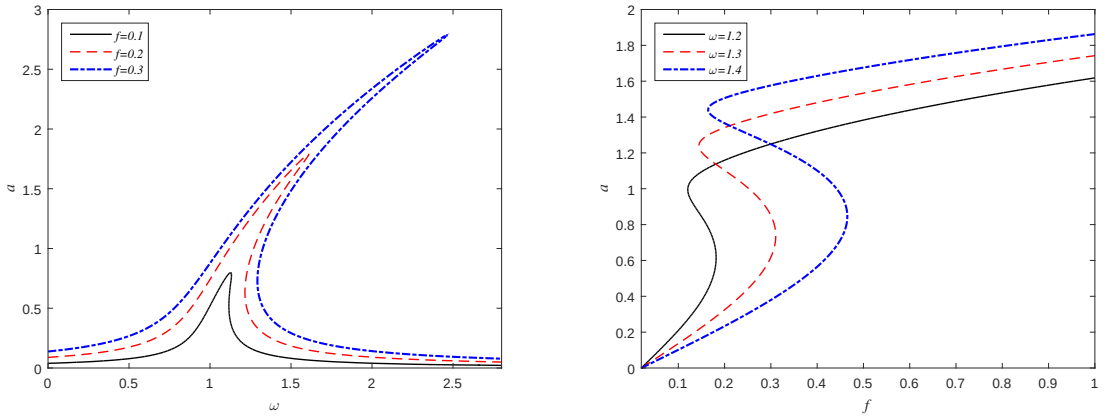

(a) (b)

Figure 4. Effect of the load fluctuation f on the amplitude-frequency curves when $\omega_0 = 1$, $d_2 = 0.5$.

This phenomenon aligns with the actual operational characteristics of spur gear transmissions: load fluctuations directly affect the dynamic meshing force between gear teeth, intensifying the alternating contact stress on the tooth surfaces. As fluctuations grow, the meshing process becomes increasingly unstable, leading to more severe impacts and vibrations during tooth engagement. This not only widens the frequency band where resonance occurs but also amplifies the amplitude of resonant vibrations, which in turn may accelerate gear wear, increase noise levels, and even reduce the overall service life of the transmission system. Thus, the observed trend in the figure underscores the critical need to mitigate excessive load fluctuations in spur gear system design and operation to ensure stable and reliable performance.

3.3. The influence of meshing stiffness fluctuations

The impact of meshing stiffness fluctuations on primary resonance is depicted in Figure 5.

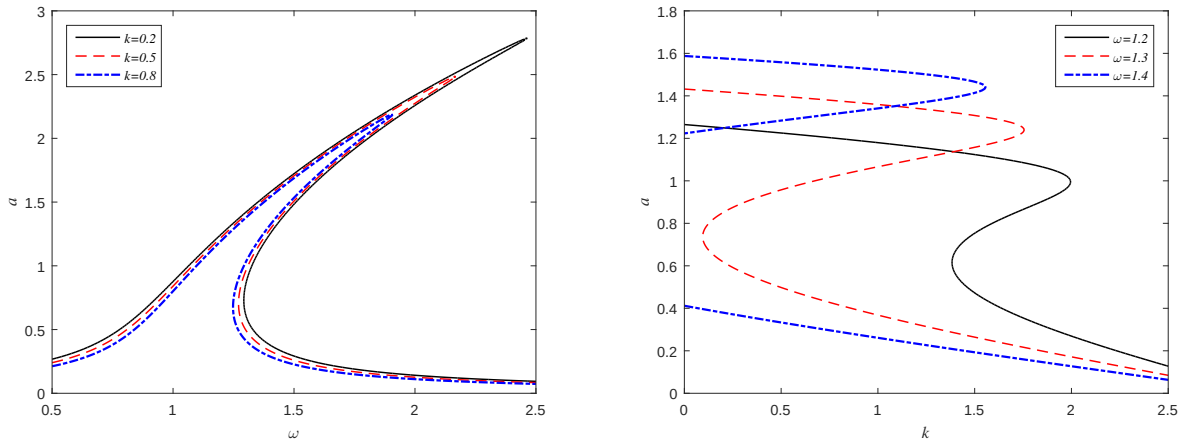

(a) (b)

Figure 5. Effect of the meshing stiffness fluctuation k on the amplitude-frequency curves when $\omega_0 = 1$, $d_2 = 0.5$.

Specifically, Figure 5(a) reveals that an increase in meshing stiffness fluctuation leads to a gradual decrease in the maximum steady-state amplitude and a corresponding shrinkage of the unstable region. This indicates that a moderate degree of stiffness fluctuation can effectively reduce the amplitude of primary resonance and enhance the stability of resonant behavior. Such effect is closely associated with dynamic tooth interaction, as controlled stiffness variations can mitigate the accumulation of vibrational energy during meshing, thereby alleviating the intensity of resonant responses and reducing the risk of excessive dynamic loads that may lead to tooth wear or structural fatigue.

Additionally, Figure 5(b) illustrates that when the excitation frequency enters the unstable region in such systems, the dynamic behavior of the gears becomes more complex, with potential for abrupt shifts in amplitude or erratic vibration patterns, and even sudden amplitude changes triggered by small meshing stiffness fluctuations. This further underscores the significance of regulating meshing stiffness fluctuations to maintain stable operation during resonant conditions.

3.4. The influence of control parameters

In spur gear transmission systems, unstable transmission can be caused by meshing damping, load fluctuations, and meshing stiffness fluctuations. To reduce system vibration and enhance operational stability, the proposed P-FDDF controller will be applied here. Figures 6–8 present the primary resonance characteristics of the spur gear system when specific control parameters change.

The effect of the proportional displacement feedback control gain on primary resonance suppression is illustrated in Figure 6. As shown in Figure 6(a), compared with the uncontrolled case, the application of proportional displacement feedback control alone does not reduce the peak amplitude of the primary resonance. Instead, it shifts the resonance skeleton curve to the right, thereby altering the frequency at which the peak amplitude occurs. Nevertheless, at a given excitation frequency ω, a certain degree of amplitude reduction can still be achieved. This is because the control introduces a linear force proportional to displacement, effectively increasing the system's stiffness. This modification changes the dynamic equilibrium, shifting the resonance frequency, but the control itself provides no energy dissipation mechanism to reduce the peak amplitude. A similar trend is observed in Figure 6(b). These results confirm that proportional displacement feedback primarily tunes the resonance frequency rather than attenuating the peak amplitude, which is consistent with its linear nature of modifying the effective stiffness without altering the system's inherent energy balance. This limitation of purely proportional control underscores the necessity of incorporating the fractional derivative term to achieve effective amplitude suppression, as demonstrated in the following analysis.

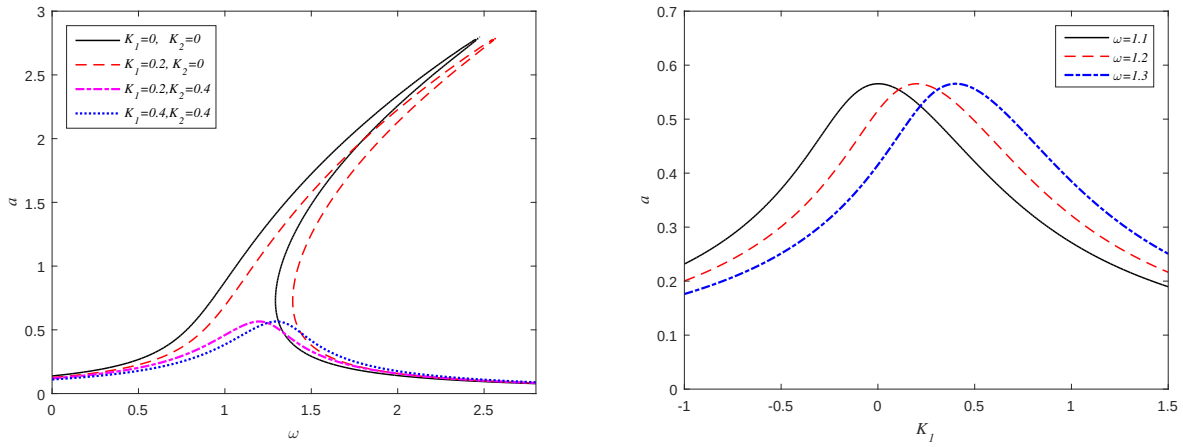

(a) (b)

Figure 6. Effect of the proportional displacement feedback gain K_1 on the amplitude-frequency curves when $q = 0.9$, $\omega_0 = 1$, $d_2 = 0.5$.

Figure 7 illustrates how the fractional derivative displacement feedback control gain K_2 affects primary resonance suppression. As observed from Figure 7(a), compared with the uncontrolled case, using this gain alone suppresses the maximum amplitude of primary resonance. A larger K_2 value reduces the steady-state amplitude more significantly, enhancing system stability. Notably, when combined with proportional displacement feedback control, this strategy both suppresses steady-state amplitude and shifts the frequency corresponding to the maximum amplitude. This synergy holds

critical importance in gear systems. The fractional-order derivative term, characterized by frequency-selective damping and energy-dissipating properties, is highly effective at attenuating resonant magnitudes and mitigating tooth meshing vibrations. Meanwhile, the proportional term complements it by tuning the resonance frequency to prevent overlap with variable meshing frequencies, which is a prevalent issue in gear system operation. Together, they tackle the dual challenges of amplitude control and frequency tuning. They overcome the limitation of fractional-order control alone, which cannot alter resonance frequency characteristics, and form a more comprehensive resonance control solution.

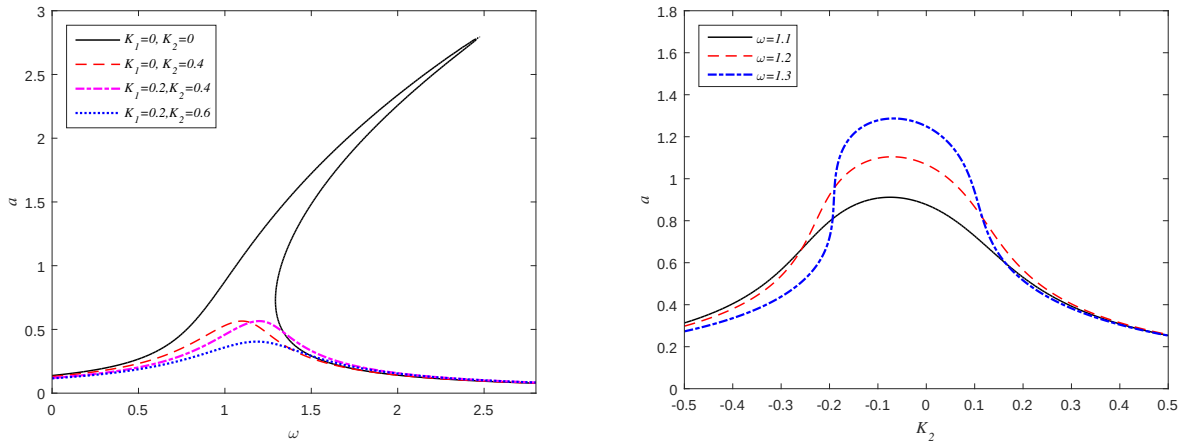

(a) (b)

Figure 7. Effect of the fractional derivative displacement feedback gain K_2 on the amplitude-frequency curves when $q = 0.9$, $\omega_0 = 1$, $d_2 = 0.5$.

Figure 7(b) shows the curves illustrating the influence of the fractional derivative displacement feedback control gain on the steady-state amplitude of primary resonance. It can be observed that when the gain K_2 takes values within a certain range, the steady-state amplitude increases. This phenomenon may occur when the phase contribution of the fractional derivative term, under inappropriate values of K_2 and q, leads to a constructive interaction with the excitation force, effectively introducing positive feedback that amplifies the vibration response instead of damping it. Consequently, in suppressing primary resonance in spur gear systems, selecting appropriate control parameters is critical to achieving effective control outcomes.

Figure 8 illustrates the effect of the order of fractional derivative displacement feedback control on primary resonance suppression. As observed from the figure, the smaller the order q, the larger the steady-state amplitude of the primary resonance, with a corresponding rightward shift of the primary resonance skeleton curve. Notably, the resonant amplitude reaches its minimum when $q = 1$. However, fractional derivative displacement feedback control (with $q \neq 1$) remains valuable in practical gear system applications. This is due to the fact that integer-order control (where $q = 1$) functions as a pure derivative action, exhibiting high sensitivity to high-frequency noise in gear meshing signals. This type of noise, originating from tooth surface imperfections or load variations, is prone to amplification, resulting in unwanted oscillations. In contrast, fractional-order control allows for flexible tuning of the order q between 0 and 1, balancing energy dissipation capacity and noise robustness. By adjusting

the fractional-order q, it can achieve near-optimal amplitude suppression while mitigating the noise amplification issue inherent to integer-order derivative control, making it a more adaptable solution for the complex, noisy operating environments of gear systems.

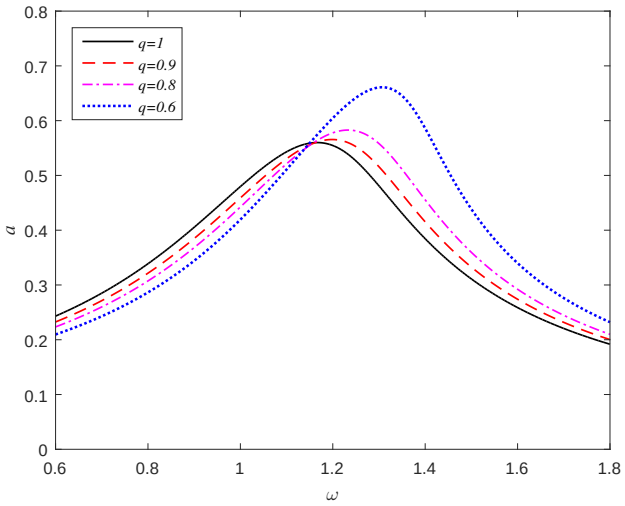

Figure 8. Effect of the fractional-order q on the amplitude-frequency curves when $\omega_0 = 1$, $d_2 = 0.5$, $K_1 = 0.2$, $K_2 = 0.4$.

3.5. Guidelines for practical parameter selection

To enhance the engineering applicability of the proposed P-FDDF controller strategy, supplementary guidelines for parameter selection are established based on the numerical analysis in Section 3.4.

The proportional gain K_1 is fundamentally correlated with resonance frequency shift, as it effectively augments the system's linear stiffness. This relationship is derived from the linearized form of the stiffness term in the amplitude-frequency response equation (2.17), where K_1 explicitly modifies the effective natural frequency of the system. For the dimensionless system with $\omega_0 = 1$, a practical operating range of $K_1 = 0.15$ to 0.3 times the square of the system's natural frequency (ω_0^2) provides sufficient frequency detuning. In practice, this ratio should be scaled according to the specific system's characteristic frequency.

The fractional derivative gain K_2 governs the damping intensity required for vibration suppression, a characteristic directly influenced by the system's load level. This relationship is reflected in the damping term of the amplitude equation, $\frac{\mu}{2} + \frac{K_2}{2}\omega_0^{q-1}\sin\frac{q\pi}{2}$. For instance, numerical results under a medium-load condition (dimensionless load amplitude $f = 0.3$) indicate effective vibration suppression with $K_2 \approx 0.1$. Accordingly, light-load gears (load amplitude below 0.2 N) employ K_2 values from 0.03 to 0.08. Medium-load gears (load amplitude between 0.2 N and 0.5 N) adopt K_2 in the range of 0.08 to 0.15. Heavy-load gears (load amplitude above 0.5 N) require K_2 values from 0.15 to 0.25 to effectively counteract resonant vibrations induced by high operational loads. Higher K_2 values under heavy loads are necessary to counteract the stronger resonant vibrations induced by substantial external excitations.

The fractional derivative order q is correlated with the meshing damping of the system, as it regulates both the frequency-dependent weighting characteristics and the memory properties of the controller. Figure 8 demonstrates that a decrease in q increases the steady-state amplitude and shifts the resonance skeleton curve. Based on the trend observed in Figure 8, where $q = 1$ yields the lowest amplitude under ideal conditions, this value serves as a theoretical benchmark for performance optimization. Nevertheless, to preserve the essential advantages of fractional-order control, such as its superior noise robustness and adaptability to complex dynamics, practical implementations should consider fractional values in the range $0.8 \leq q < 1$. This approach retains the frequency-weighting benefits of fractional calculus while still providing adequate vibration suppression. It thus represents an optimal balance between theoretical performance and the practical requirements of general-purpose transmission systems.

4. Time history and phase diagram analysis

To further validate the dynamic characteristics of the spur gear system under the P-FDDF controller, time history curves and phase portraits (displacement vs. velocity) are analyzed to visualize transient and steady-state behaviors. These analyses complement the amplitude-frequency response results from Section 3. They reveal the system's temporal evolution and stability transitions, thereby providing a more comprehensive understanding of how control parameters and operational perturbations influence dynamic performance.

To establish a baseline for evaluating the P-FDDF controller's effectiveness, a numerical investigation was carried out to explore the dynamic behavior of a spur gear transmission system subjected to different parameter perturbations, with a specific focus on the system response in the absence of active control measures. As illustrated in Figure 9, the simulation encompasses three distinct operational scenarios that mirror realistic variations in loading and stiffness conditions encountered in practical gear applications. System parameters were configured in line with the dimensionless mathematical model presented in Eq (2.1) of this paper, with key values set as follows: $\mu = 0.1$, $d_1 = 1$, $d_2 = 0.5$, $f_0 = 0.1$, $f = 0.3$, and $k = 0.2$. The simulation employed MATLAB's ode45 solver, with a time span of 0 to 20 seconds and a time step of 0.01 seconds, to ensure accurate capture of both transient and steady-state dynamic responses of the system.

Three critical operational conditions were analyzed: A normal operating condition with baseline parameters ($f = 0.3, k = 0.2$) shown in blue; a large-load disturbance condition with dynamic load amplitude $f = 0.6$ (100% increase) shown in red; and a large stiffness fluctuation condition with stiffness fluctuation amplitude $k = 0.5$ (150% increase) shown in green. The time-domain responses in Figure 9(a) demonstrate that the normal condition exhibits stable periodic oscillations with amplitudes of approximately ±0.1, the large-load disturbance condition shows increased amplitudes of approximately ±0.15, and the large stiffness fluctuation condition maintains similar amplitude levels with modified oscillation patterns. The corresponding phase portraits in Figure 9(b) were generated using data points collected after the initial 60% of simulation duration to characterize steady-state behavior, effectively eliminating transient effects. All three conditions generate closed limit cycles, confirming the existence of stable periodic solutions. The expansion of limit cycles under parameter perturbations indicates increased oscillatory energy while maintaining structural stability. The analysis verifies that the uncontrolled gear system retains its fundamental periodic nature under substantial

parameter variations. However, it also demonstrates the system's vulnerability to load and stiffness fluctuations, highlighting an urgent need for an effective active controller to counteract such adverse effects.

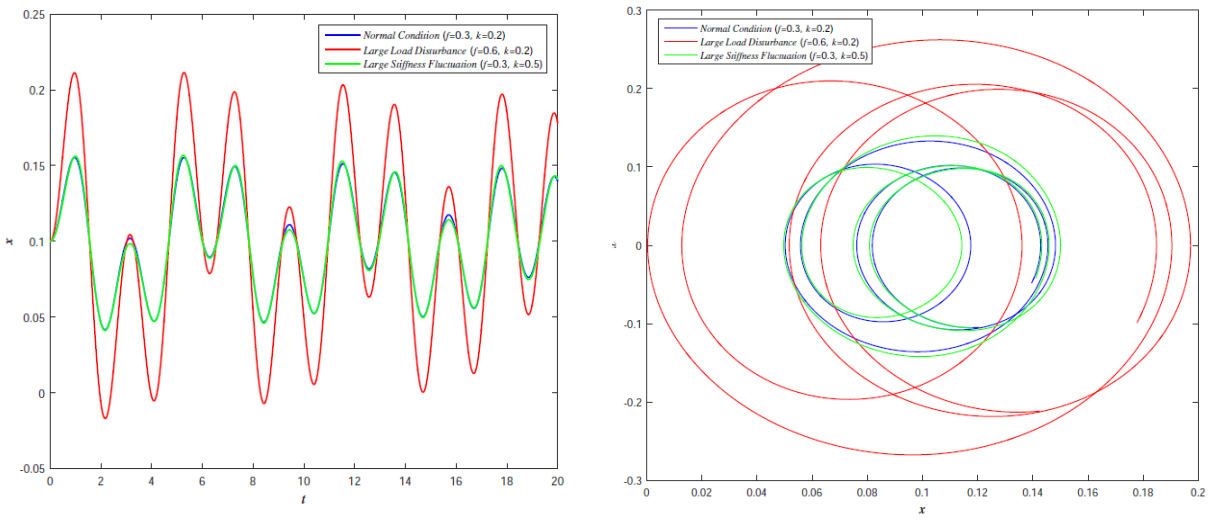

(a) (b)

Figure 9. Dynamic behavior subjected to different parameter perturbations: (a) time responses, (b) corresponding phase portraits.

Building directly on the baseline analysis of the uncontrolled system, Figure 10 presents the dynamic response of a spur gear system under P-FDDF control ($K_1 = 0.2, K_2 = 0.4, q = 0.9$) for three operational conditions: Normal ($f = 0.3, k = 0.2$), large load disturbance ($f = 0.6, k = 0.2$), and large stiffness fluctuation ($f = 0.3, k = 0.5$). Figure 10(a) shows the time-domain displacement responses. The normal condition exhibits regular periodic oscillations. The load disturbance condition demonstrates increased amplitude response due to 100% higher dynamic excitation. The stiffness fluctuation condition shows comparable amplitudes but modified oscillation patterns, indicating the controller's adaptation to parameter variations. Figure 10(b) displays the corresponding phase portraits. All three conditions produce closed limit cycles, confirming stable periodic behavior. The red cycle (load disturbance) expands notably compared to the blue baseline, reflecting increased oscillatory energy. The green cycle (stiffness fluctuation) shows shape distortion, representing altered system dynamics under stiffness variation. This direct comparative analysis demonstrates that the P-FDDF controller effectively mitigates parameter perturbations: it maintains small-amplitude, stable periodic motion across all tested conditions, outperforming the uncontrolled system by reducing oscillation energy and enhancing dynamic stability.

To further isolate and quantify the resonance suppression effect of the P-FDDF controller, Figure 11 compares the time history responses of the uncontrolled and controlled systems under identical operating parameters. The blue curve corresponds to the uncontrolled system with parameters $q = 0.9$, $\mu = 0.1$, $k = 0.2$, $f_0 = 0.1$, $f = 0.3$, $\omega = 1.2$, $\omega_0 = \sqrt{d_1} = 1$, $d_2 = 0.5$.

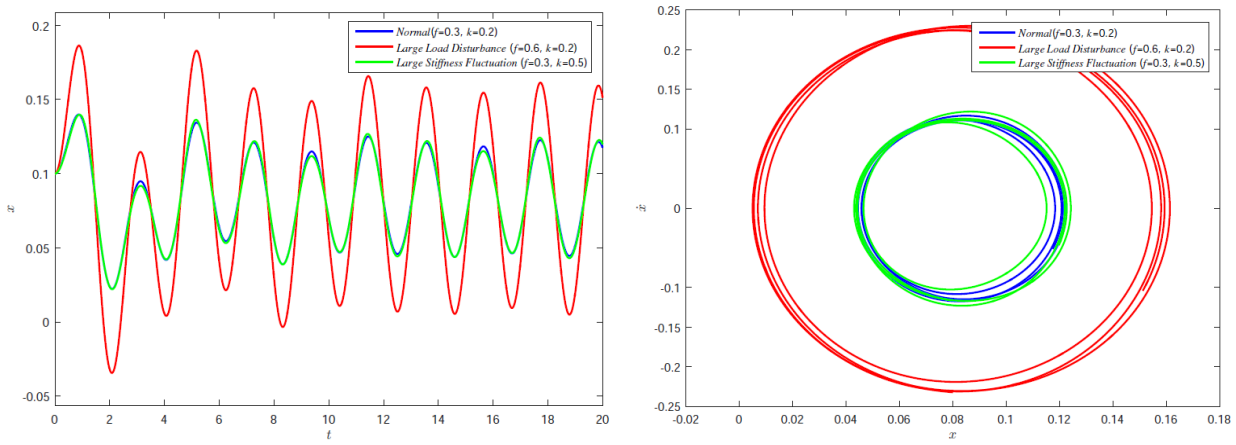

(a) (b)

Figure 10. P-FDDF controlled system response: (a) time responses under different working conditions, (b) corresponding phase portraits.

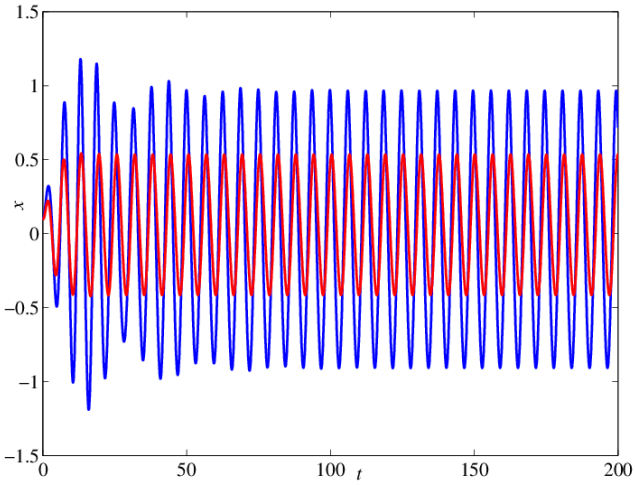

Figure 11. Time history responses of the controlled and uncontrolled systems.

This curve exhibits large-amplitude oscillations with sustained fluctuations, indicating strong resonant vibrations caused by time-varying meshing stiffness and fluctuating loads. In comparison, the system under P-FDDF control with gain parameters $K_1 = 0.2, K_2 = 0.4$, represented by the red curve, shows a notable improvement in dynamic performance. The time history response of the controlled system demonstrates a rapid decay of transient vibrations, quickly converging to a steady-state amplitude of about 0.5. This swift stabilization underscores the efficacy of the fractional-order derivative term in dissipating vibrational energy.

Complementing the time history analysis, the corresponding phase portraits provide deeper insight into the system's dynamic stability mechanisms. In the uncontrolled case, shown in Figure 12(a), the trajectory is scattered and non-convergent, forming multiple irregular loops. This pattern signifies chaotic dynamics and inherent instability, which aligns with the previously observed multi-valued

amplitude phenomenon and confirms the system's inability to attain a stable steady state without control. In contrast, the phase portrait under P-FDDF control, presented in Figure 12(b), reveals a distinct transformation into a compact and well-defined closed limit cycle. This clear periodic orbit demonstrates the successful suppression of resonance and a significant enhancement of the system's overall stability.

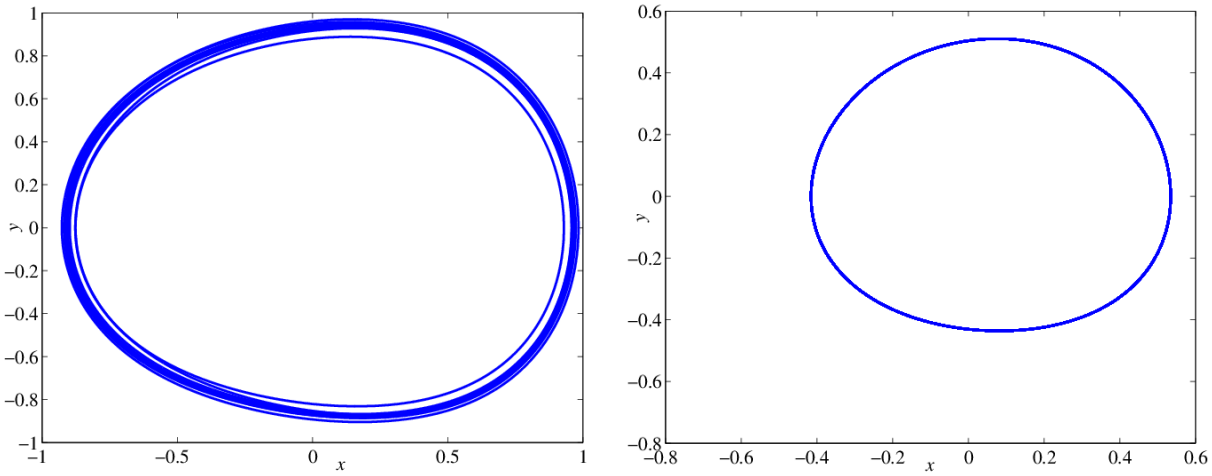

(a) (b)

Figure 12. Phase portraits of the uncontrolled and controlled systems.

Finally, to investigate how adjustments to control parameters influence the controller's performance, Figure 13 illustrates the time history responses of the system under two distinct control parameter sets. The blue curve, corresponding to the case with control gains set to $K_1 = 0.2$ and $K_2 = 0.4$, exhibits a steady-state oscillation with a relatively large amplitude. In contrast, the red curve represents the controlled system with gains $K_1 = 0.4$ and $K_2 = 0.4$. This configuration results in a significant reduction in the vibration amplitude while maintaining a stable periodic response. The comparison clearly demonstrates that increasing the K_1 gain effectively suppresses the system's oscillatory response, leading to improved dynamic performance.

In summary, the time history and phase diagram analyses demonstrate the superior performance of P-FDDF control. It effectively suppresses the large-amplitude vibrations characteristic of the uncontrolled system, ensuring rapid convergence to a stable, low-amplitude steady state. This behavior, visualized as a compact limit cycle, provides comprehensive validation of the control's ability to mitigate primary resonance in spur gear systems. Compared with the prior study in [10] that utilized time-delay feedback control, a method often associated with stability limitations and constrained adaptability in strongly nonlinear regimes, the present work introduces a proportional-fractional-derivative feedback controller. This approach effectively suppresses resonant amplitudes while tuning the system frequency, leveraging the complementary actions of proportional control and fractional-order damping, the latter offering frequency-dependent weighting and memory effects. The study also corrects analytical inaccuracies in earlier amplitude-frequency equations, supplies practical parameter selection guidelines tailored to distinct operational conditions, and demonstrates enhanced control performance through comprehensive numerical simulations under various perturbation scenarios.

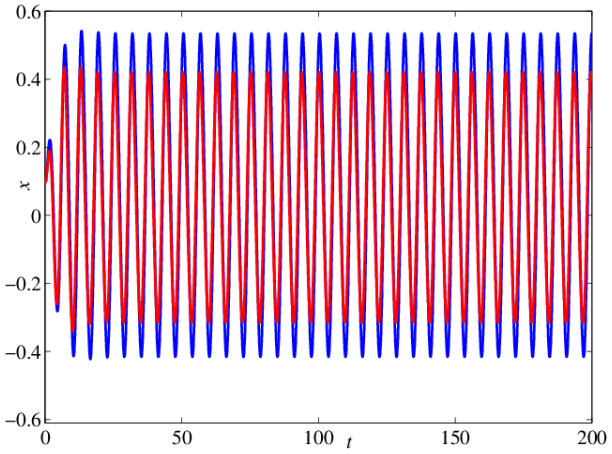

Figure 13. Time responses under different control parameters.

5. Conclusions

This study establishes a comprehensive solution for primary resonance suppression in nonlinear spur gear systems through the proposed P-FDDF controller. The developed dynamic model incorporates essential nonlinearities including time-varying stiffness and backlash effects, while the multiple scale analysis provides a theoretical foundation for amplitude-frequency characteristics prediction. Stability analysis verifies that control parameters can effectively enhance system stability. Numerical results reveal that increased meshing damping effectively diminishes the amplitude of primary resonance, while greater load fluctuations amplify vibrational responses and expand the resonance range. Meanwhile, meshing stiffness fluctuations exert a dual influence on system stability: Moderate fluctuations reduce steady-state resonance amplitudes and shrink unstable regions, whereas excessive or erratic fluctuations can trigger abrupt amplitude shifts and complicate dynamic behavior.

The efficacy of P-FDDF control is further confirmed through time history analyses and phase portraits, which illustrate significant reduction in vibration amplitude and improved stability. Uncontrolled systems exhibit persistent large-amplitude vibrations with irregular, non-convergent trajectories in phase portraits, reflecting unstable dynamics. In contrast, under P-FDDF control, time history curves show rapid attenuation of transient vibrations, converging to small steady-state amplitudes, and phase portraits form compact, closed limit cycles, indicating stable periodic motion. These visualizations confirm that the control strategy not only suppresses resonant amplitudes but also accelerates the system's transition to a steady state, reinforcing its effectiveness in stabilizing complex gear dynamics.

In terms of control strategies, the P-FDDF controller achieves excellent performance by leveraging its proportional term to tune resonance frequency and its fractional-order derivative term to suppress amplitudes, addressing both amplitude-related and frequency-related issues. This research corrects previous analytical errors in the amplitude-frequency response equations [10, 20], and offers insights into how key parameters (e.g., meshing stiffness, control gains) influence the system.

Author contributions

Zhongyang Su performed the writing of the original draft and the review and editing; Zhoujin Cui performed the conceptualization, methodology, validation, supervision, and writing—review and editing; Hanlin Huang performed the investigation and validation. All authors have read and approved the final version of the manuscript for publication.

Use of Generative-AI tools declaration

The authors declare they have not used Artificial Intelligence (AI) tools in the creation of this article.

Acknowledgments

The authors express gratitude to the reviewers and editors for their helpful comments and suggestions, as well as to the financial support from the High Level Talent Research Launch Fund of Jiangsu Second Normal University (No. 928201/058) and the Excellent Grassroots Teaching Organization Project of Jiangsu Second Normal University (No. 742401/011).

Conflict of interest

All authors declare no conflicts of interest in this paper.

References

1. S. P. Radzevich, *Theory of gearing: Kinematics, geometry, and synthesis*, 3 Eds., CRC Press, 2022. https://doi.org/10.1201/9781003311744
2. S. P. Radzevich, *Recent advances in gearing*, Switzerland: Springer Cham, 2022. https://doi.org/10.1007/978-3-030-64638-7
3. M. Faggioni, F. S. Samani, G. Bertacchi, F. Pellicano, Dynamic optimization of spur gears, *Mech. Mach. Theory*, **46** (2011), 544–557. https://doi.org/10.1016/j.mechmachtheory.2010.11.005
4. A. Kahraman, R. Singh, Non-linear dynamics of a spur gear pair, *J. Sound Vib.*, **142** (1990), 49–75. https://doi.org/10.1016/0022-460x(90)90582-k
5. A. Kahraman, R. Singh, Interactions between timevarying mesh stiffness and clearance non-linearities in a geared system, *J. Sound Vib.*, **146** (1991), 135–156. https://doi.org/10.1016/0022-460x(91)90527-q
6. A. Kahraman, R. Singh, Non-linear dynamics of a geared rotor-bearing system with multiple clearances, *J. Sound Vib.*, **144** (1991), 469–506. https://doi.org/10.1016/0022-460x(91)90564-z
7. I. Howard, S. Jia, J. Wang, The dynamic modelling of a spur gear in mesh including friction and a crack, *Mech. Syst. Signal Pr.*, **15** (2001), 831–853. https://doi.org/10.1006/mssp.2001.1414
8. G. Liu, R. G. Parker, Dynamic modeling and analysis of tooth profile modification for multimesh gear vibration, *J. Mech. Design*, **130** (2008), 1–13. https://doi.org/10.1115/1.2976803

9. G. Liu, R. G. Parker, Nonlinear dynamics of idler gear systems, *Nonlinear Dynam.*, **53** (2008), 345–367. https://doi.org/10.1007/s11071-007-9317-z
10. Y. Yang, M. Xu, Y. Du, P. Zhao, Y. P. Dai, Dynamic analysis of nonlinear time-varying spur gear system subjected to multi-frequency excitation, *J. Vib. Control*, **25** (2019), 1210–1226. https://doi.org/10.1177/1077546318814951
11. H. Moradi, H. Salarieh, Analysis of nonlinear oscillations in spur gear pairs with approximate modeling backlash nonlinearity, *Mech. Mach. Theory*, **51** (2012), 14–31. https://doi.org/10.1016/j.mechmachtheory.2011.12.005
12. C. I. Park, Dynamic behavior of the spur gear system with time varying stiffness by gear positions in the backlash, *J. Mech. Sci. Technol.*, **34** (2020), 565–572. https://doi.org/10.1007/s12206-020-0104-9
13. J. Zhao, L. Hou, Z. Q. Li, H. Zhang, R. P. Zhu, Prediction of tribological and dynamical behaviors of spur gear pair considering tooth root crack, *Eng. Fail. Anal.*, **135** (2022), 106145. https://doi.org/10.1016/j.engfailanal.2022.106145
14. A. Celikay, A. Donmez, A. Kahraman, An experimental and theoretical study of subharmonic resonances of a spur gear pair, *J. Sound Vib.*, **515** (2021), 116421. https://doi.org/10.1016/j.jsv.2021.116421
15. J. Z. Ye, J. Wei, A. Q. Zhang, S. L. Chen, T. Ran, R. Z. Shu, Theoretical and experimental study on the dynamic behavior of spur gear transmission system during hovering maneuver flights, *Mech. Syst. Signal Pr.*, **212** (2024), 111296. https://doi.org/10.1016/j.ymssp.2024.111296
16. M. H. Chen, M. J. Brennan, Active control of gear vibration using special integrated sensors and actuators, *Smart Mater. Struct.*, **9** (2000), 342–350. https://doi.org/10.1201/9781482268560-16
17. M. F. Li, T. C. Lim, W. S. Shepard, Y. H. Guan, Experimental active vibration control of gear mesh harmonics in a power recirculation gearbox system using a piezoelectric stack actuator, *Smart Mater. Struct.*, **14** (2005), 917–927. https://doi.org/10.1088/0964-1726/14/5/028
18. S. Liu, S. Zhao, B. Niu, J. X. Li, H. B. Li, Stability analysis of a nonlinear electromechanical coupling transmission system with time delay feedback, *Nonlinear Dynam.*, **86** (2016), 1863–1874. https://doi.org/10.1007/s11071-016-3000-1
19. H. B. Li, J. J. Hu, Y. T. Shi, S. Liu, Dynamic behavior analysis and time delay feedback control of gear pair system with backlash non-smooth characteristic, *J. Vibroeng.*, **19** (2017), 302–313. https://doi.org/10.21595/jve.2016.17157
20. H. Shi, D. Zhao, Z. Li, Primary resonance analysis for a spur gear system with time delay feedback control, *J. Vib. Shock*, **38** (2019), 91–96.
21. Z. Yue, Y. Wang, Z. Chen, G. Yu, L. Pavel, Z. Michael, et al., Resonance and stability of piezoelectric Herringbone gears under time-delay feedback, *Appl. Math. Model.*, **147** (2025), 116216. https://doi.org/10.1016/j.apm.2025.116216
22. H. S. Bauomy, A. T. EL-Sayed, Oscillation controlling in nonlinear motorcycle scheme with bifurcation study, *Mathematics*, **13** (2025), 3120. https://doi.org/10.3390/math13193120
23. A. Alanazy, A. T. EL-Sayed, F. T. El-Bahrawy, A non-perturbative methodology for a cantilever-beam dynamical system with bifurcation and negative derivative feedback controlling, *AIMS Math.*, **10** (2025), 17832–17867. https://doi.org/10.3934/math.2025795

24. Y. Shen, J. Niu, S. Yang, S. Li, Primary resonance of dry-friction oscillator with fractional-order Proportional-Integral-Derivative controller of velocity feedback, *J. Comput. Nonlinear Dyn.*, **11** (2016), 051027. https://doi.org/10.1115/1.4033443
25. J. Chen, X. Li, J. Tang, Y. Liu, Primary resonance of van der Pol oscillator under fractional-order delayed feedback and forced excitation, *Shock Vib.*, **2017** (2017), 5975329. https://doi.org/10.1155/2017/5975329
26. L. Liu, J. C. Niu, X. H. Li, Dynamic analysis of gear system under fractional-order PID control with the feedback of meshing error change rate, *Acta Mech.*, **229** (2018), 3833–3851. https://doi.org/10.1007/s00707-018-2194-3
27. L. Marinangeli, F. Alijani, S. H. HosseinNia, Fractional-order positive position feedback compensator for active vibration control of a smart composite plate, *J. Sound Vib.*, **412** (2018), 1–16. https://doi.org/10.1016/j.jsv.2017.09.009
28. H. Yan, Q. Ma, J. Wang, H. Huang, Fractional-order time-delay feedback control for nonlinear dynamics in giant magnetostrictive actuators, *Nonlinear Dynam.*, **112** (2024), 3055–3079. https://doi.org/10.1007/s11071-023-09228-6
29. M. N. A. El-Salam, R. K. Hussein, Reducing the primary resonance vibrations of a cantilever beam using a proportional fractional-order derivative controller, *Mathematics*, **13** (2025), 1886. https://doi.org/10.3390/math13111886
30. A. H. Nayfeh, *Perturbation methods*, New York: John Wiley & Sons, 2000. https://doi.org/10.1002/9783527617609
31. A. H. Nayfeh, D. T. Mook, *Nonlinear oscillations*, New York: Wiley-Interscience, 1995. https://doi.org/10.1002/9783527617586
32. A. H. Nayfeh, *Introduction to perturbation techniques*, New York: John Wiley & Sons, 1981. https://doi.org/10.1137/1024080
33. Z. J. Cui, Z. H. Wang, Primary resonance of a nonlinear fractional model for cerebral aneurysm at the circle of Willis, *Nonlinear Dynam.*, **108** (2022), 4301–4314. http://dx.doi.org/10.1007/s11071-022-07445-z
34. Z. J. Cui, X. R. Zhang, W. Zong, Superharmonic resonance analysis and time-delay feedback controllability of a forced fractional Mathieu-Duffing equation, *Mediterr. J. Math.*, **22** (2025), 219. https://doi.org/10.1007/s00009-025-02989-x
35. Z. J. Cui, X. R. Zhang, T. Lu, Resonance analysis and time-delay feedback controllability for a fractional horizontal nonlinear roller system, *AIMS Math.*, **9** (2024), 24832–24853. https://doi.org/10.3934/math.20241209
36. J. P. Lasalle, *The stability of dynamical systems*, Phila: Society for Industrial and Applied Mathematics, 1976. https://doi.org/10.1137/1.9781611970432

AIMS Press